arXiv:1911.02784v1 [physics.geo-ph] 7 Nov 2019

Comparison of AATR and WTEC indices in the studies of the level of ionospheric disturbance

Berngardt O.I., Voeykov S.V., Perevalova N.P.

Institute of Solar-Terrestrial Physics SB RAS, 126a, Lermontova Str., Irkutsk, Russia 664033

Abstract

A comparative statistical analysis of AATR and WTEC indices was conducted based on data from the ISTP SB RAS GNSS receivers network. It is shown that at high levels of ionospheric disturbance (for WTEC $>$ 0.1 TECU), the AATR index is proportional to the WTEC index with a factor of $1.5 min^{-1}$. At small levels of ionospheric disturbance (for WTEC $<$ 0.1 TECU), this proportionality is violated. It is shown that the contribution of daily dynamics of the background ionosphere to the AATR index is higher than to the WTEC index. This leads to a higher sensitivity of the WTEC index to disturbances. This also leads to violating the proportionality between WTEC and AATR indices at low levels of ionospheric disturbance. It is shown that at high latitudes the dynamics of the WTEC and AATR indices correlate significantly with the level of geomagnetic disturbance Kp. At mid-latitudes, the contribution of solar radiation variations (F10.7 index) and vertical seismic variations exceeds the influence of Kp variations. The program for calculating WTEC indices, used in the paper is put into open access.

Keywords: GPS TEC; ionosphere; ionospheric disturbances; AATR index; WTEC index

Email address: berng@iszf.irk.ru,serg3108@iszf.irk.ru,pereval@iszf.irk.ru (Berngardt O.I., Voeykov S.V., Perevalova N.P.)

1. Introduction

The ionosphere and the ionospheric disturbances have a significant impact on Global Navigation Satellite Systems (GNSS). Dense worldwide networks of GNSS receivers and their high temporal resolution make it possible to monitor the ionospheric conditions in real time using Slant Total Electron Content (STEC) calculated along the line-of-sight (LOS) between transmitting GNSS satellite and GNSS receiver.

The methods of studying the ionosphere using GNSS receivers can be divided into two large groups - techniques for using a single receiver, and techniques for using a network of receivers (global or local). In the case of using a network, it becomes possible to study large-scale irregularities and their large-scale spatial variations, based on the production of total electron content (TEC) maps: GIM (Mannucci et al., 1998; CDDIS, 2019) and TEC disturbance maps (TDM) (Perevalova et al., 2008; Afraimovich, E.L. et al., 2013). The first index (index of TEC perturbations) built based on GIM was proposed by (Ho et al., 1998). Later W and Wp indices have been developed (Gulyaeva and Stanislawska, 2008; Gulyaeva et al., 2013; Stanislawska and Gulyaeva, 2015). Using GIM allows one to distinguish the perturbed part in the world-wide distribution of TEC - nearly static and global-scale. TDM allows one to to study wave-like disturbances associated with the passage of different irregularities of different scales (Astafyeva and Shults, 2018). Joint analysis of network of receivers allows one to use radio tomographic methods to determine the spatial characteristics of irregularities and to build special indices based on them (HORT IPI (Nesterov et al., 2017)) or use spatio-temporal combinations of their data, like DIX (Jakowski et al., 2012b,a), GIX and SIDX(Jakowski and Hoque, 2019), DIXSG(Wilken et al., 2018) and RIDX (Stankov et al., 2006) indices.

.

Statistical parameters of mid- and small-scale irregularities can be estimated using even a single GNSS receiver. Using single receivers is useful when one have rarefied network, and minimizes the obtaining and data processing efforts.

Classical index for studying ionospheric irregularities is scintillation index S4, that is regularly measured by GNSS receivers(Béniguel et al., 2004). The S4 index is usually associated with small-scale irregularities, comparable with the Fresnel radius, and leading to phase and amplitude distortions of the received signal.

To study larger ionospheric irregularities that do not significantly distort the signal shape, one use the construction of various integral indices based on variations of the measured signal phase and group delays and characterized by STEC. STEC-based indices include IROT (Wanninger, 1993), ROTI(Pi et al., 1997), fp and Fp (Mendillo et al., 2000), AATR (Sanz et al., 2014; Juan et al., 2018), WTEC(Voeykov et al., 2016). The use of STEC-based indices looks more reasonable for analysis of mid-scale irregularities than S4.

In the quiet mid-latitude ionosphere one of the sources of mid-scale irregularities are acoustic waves, generated by different sources: earthquakes (Astafyeva and Shults, 2018), meteorites(Berngardt et al., 2015), typhoones (Polyakova and Perevalova, 2013), solar terminator (Afraimovich et al., 2009), rocket launches (Kakinami et al., 2013; Zherebtsov and Perevalova, 2019) and others.

Indices ROTI and AATR are traditional ones and can be used for checking the effectiveness of other indices.

The ROTI index (Rate Of Change Of The TEC) has been used for monitoring of mid-scale ionospheric disturbances for a long time (Pi et al., 1997). ROTI is defined as the Root Mean Square error (RMS) of the Rate of Change of the TEC (ROT) at a certain time interval (usually 5 min) at single beam "satellite-receiver" and therefore has local spatial character. A strong positive correlation between GNSS positioning error and ROTI for receivers located above 64^oN (Jacobsen and Dähnn, 2014) allows using it to estimate GNSS positioning errors at high-latitudes. High values of ROTI index during severe geomagnetic storms in 2014-2015 (Jacobsen and Andalsvik, 2016; Cherniak et al., 2018) allows using this index to monitor the activity of mid-scale ionospheric irregularities at high- and low-latitudes using single GNSS-receiver (Pi et al., 1997).

The AATR (Along Arc TEC Rate) index characterizes the average level of

ionospheric disturbances over wide spatial region, measured by single GNSS-receiver (Sanz et al., 2014; Juan et al., 2018). Using AATR index is effective when one need to skip spatial dependence of ROTI. In practice the AATR index is defined as ROT averaged over a selected time interval (usually over 1 hour) and averaged over all GNSS satellites visible at the single receiver. The effective size of the area used for index estimation is defined by relative positions of the GNSS receiver and GNSS satellites. At middle latitudes this size has radius about 1500–2000 km. AATR is sensitive to the regional behavior of the ionosphere and can be used to identify the conditions where a degradation in user performance is expected (Sanz et al., 2014).

The WTEC (Variations of Vertical TEC) index (Voeykov et al., 2016) allows one to estimate the integral intensity of ionospheric disturbances of various scales at single GNSS receiver. The WTEC index represents the amplitude of variations of vertical TEC filtered in a selected range of periods and averaged over all the satellites visible by single GNSS receiver. WTEC temporal resolution is determined by the temporal resolution of the GNSS receiver and usually about 30 s. Based on WTEC analysis (Perevalova et al., 2016) revealed the features of large- and medium-scale TEC disturbances in mid-latitude and high-latitude regions. Using WTEC for mid-scale disturbances, the ionospheric effects of the Chelyabinsk meteorite fall on February 15, 2013 are studied (Voeykov et al., 2016).

Due to AATR and WTEC are calculated over approximately the same ionospheric area but by different algorithms, their efficiency can be effectively compared for their practical usage. In this paper, we performed an analysis of AATR and WTEC indices to compare their efficiency for studying mid-scale ionospheric disturbances in different conditions and geographical locations. The analysis was carried out using the data of high-latitude, equatorial and mid-latitude GNSS receivers during 2014-2017.

2. Calculation of AATR and WTEC

The initial data for determining the AATR and WTEC indices are the time series $I(t)$ of the Slant TEC along LOS and the time series $\theta(t)$ of the GNSS satellite elevation angles. We calculated STEC based on dual-frequency phase measurements at the GNSS receiver by using standard method (Hofmann-Wellenhof et al., 2001). STEC is measured in TECU (Total Electron Content Unit): $1TECU = 10^{16} el/m^2$. The elevation angles are taken from the GNSS navigation messages.

The values and dynamics of the AATR and WTEC indices can be significantly distorted by gaps in phase measurements at GNSS receiver: missing samples and cycle-slips. The both algorithms includes a preliminary detection and removal of the data with gaps before calculating the indices. The gaps can be associated with the temporary loss of the satellite signal at GNSS receiver, as well as with a small signal-to-noise ratio. The information about missing samples is taken directly from the GNSS receiver data by using Lost of Lock Indicator (LLI) (IGS and RTCM-SC104, 2015). A cycle-slip is a change of measured signal phase by an integer number of wavelengths. Several techniques have been developed for detecting cycle-slips (Hofmann-Wellenhof et al., 2001; Juan et al., 2018). In this paper, we detect the cycle-slip as the cases when the absolute value of the second derivative of STEC for consecutive samples exceeded a threshold value. The threshold is a constant determined individually for each GNSS receiver used in the paper, it is based on the several years of observations and is about $17 - 26\,TECU/min^2$. In the paper we use only continuous data series without gaps, with a duration of at least 20 minutes. To reduce the influence of the low-elevation refraction effects we use only the data at high elevation angles exceeding 15^o (Voeykov et al., 2016). Selected data series have been used for calculating AATR and WTEC.

The algorithm for AATR calculation is described in detail in (Sanz et al., 2014; Juan et al., 2018) and includes the following operations. Over the continuous data series we calculate the rate of the STEC variation (ROT_k^j) between

two consecutive samples, received from j-th satellite during k-th epoch (t_k). Instantaneous $AATR_k^j$ is calculated as ROT_k^j multiplied by a slant factor M_k^j to convert the slant TEC to vertical TEC. In the approximation of a thin ionospheric layer M_k^j depends on the ionospheric layer height h_{max} and on the satellite elevation θ_k^j. AATR index is calculated as the Root Mean Square (RMS) of the instantaneous $AATR_k^j$ over all the visible satellites during the selected time interval (1 hour). AATR index is measured in TECU/min with the temporal resolution 1 hour.

The algorithm for WTEC calculation is described in detail in (Voeykov et al., 2016) and includes the following operations. The continuous STEC series $I_k^j(t)$ for each j-th satellite and k-th epoch are transformed into vertical TEC using a slant factor M_k^j in the thin spherical ionosphere approximation. The obtained vertical TEC series are filtered by a moving-average method to provide filtered series $dI_k^j(t)$ with periods less than T minutes. The average intensity of TEC oscillations $A_k^j(t)$ is calculated as average absolute value of $dI_k^j(t)$ over T minutes period. $WTEC_k$ index for a given epoch t_k is calculated as the weighted average of the $A_k^j(t)$ series over all the visible satellites. Weighting function is specially chosen to provide smooth estimate of WTEC values, not depending on number of visible satellites. The resulting continuous $WTEC(t)$ series reflect the average level of vertical TEC variations near the selected station. WTEC is measured in TECU. Its temporal resolution is defined by the temporal resolution of the GNSS receiver (30 seconds). In the paper, we use T=10min that corresponds to mid-scale TEC disturbances. It should be noted that the period of TEC variations is closely related to the spatial scale of the ionospheric disturbances: large-scale (LS) disturbances in the ionosphere have periods of more than 30 minutes and size above 600 km, irregularities with periods of 5–20 minutes and sizes of 50–600 km are usually considered as medium-scale (MS) disturbances, small-scale (SC) disturbances have periods less than 5 min and sizes less than 30 km(Hargreaves, 1992).

To make a joint analysis of AATR and WTEC indices, we produced the software that calculates both the AATR and WTEC indices based on the algo-

rithms described in (Sanz et al., 2014; Juan et al., 2018; Voeykov et al., 2016) and use the same data sets without gaps for the calculations. The program we developed is available at (Voeykov and Berngardt, 2019). For the comparison with AATR series the WTEC series are decimated to 1 hour temporal resolution. As showed the analysis below, the released AATR calculation algorithm produces the values similar to the results of (Sanz et al., 2014). This allows us to verify our program and use it for the joint analysis of WTEC and AATR indices.

3. Experimental data

For a comparative analysis of AATR and WTEC indices the data from midlatitude, high-latitude and low-latitude GNSS receivers are used. Their locations are shown in Fig.1. The low-latitude GNSS stations NTUS, BOGT and BRAZ are the part of International GNSS Service (IGS) network (IGS, 2019). These low-latitude stations are chosen to provide compatibility of this work with (Sanz et al., 2014). Midlatitude ISTP SB RAS Baikal network (SibNet) of GNSS receivers (Ishin et al., 2017) is shown in Fig.1B and includes 10 receivers (ORDA, UZUR, SARM, MKSM, ISTP, LIST, MOND, TORA, TORB, TORC). In Fig.1A SibNet is marked as 'ISTP'. Also for analysis we use the data of high-latitude NORI receiver of ISTP SB RAS. Below we present results of comparative statistical analysis of AATR and WTEC dynamics over the period 2014-2017 using GNSS data and the algorithms described above. We also present results of regression analysis of AATR and WTEC with parameters of solar, geomagnetic and seismic activity as well as with background total electron content. We also demonstrate AATR and WTEC sensitivity to strong and weak ionospheric disturbances generated by geomagnetic storms and earthquakes correspondingly.

The following solar and geophysical data were used for the analysis:

- the geomagnetic indices Kp, Dst, SYM-H obtained from Kyoto World Data Center for Geomagnetism (WDC, 2019) and OMNIWeb database(OMNIWeb,

2019);

- the vertical total electron content (VTEC), characterizing the background ionospheric conditions obtained from Global Ionosphere Maps (GIM) produced by Center for Orbit Determination in Europe (CODE). The CODE GIMs were obtained from the Crustal Dynamics Data Information System (CDDIS) at Goddard Space Flight Center, NASA(CDDIS, 2019);

- the F10.7 index of solar radiation at 10.7 cm wavelength, maximal over 1 hour and obtained from OMNIWeb database (OMNIWeb, 2019);

- the vertical seismic variation (dZ) according to the data of Talaya seismic station (TLY) maximal over 1 hour and obtained from the IRIS (Incorporated Research Institutions for Seismology) database(IRIS, 2019). TLY seismic station is located near the GNSS receiver TORA.

Statistical analysis of the indices Fig.2 shows WTEC and AATR indices at high-latitude (Fig.2A-B), mid-latitude (Fig.2C-H) and equatorial (Fig.2I-N) GNSS stations. For the analysis of equatorial station data we use the days 070-074 of 2013, studied in detail in (Sanz et al., 2014) over the identical set of low-latitude stations. Comparison of Fig.2I-N with results of (Sanz et al., 2014, ,fig.10) shows a good agreement between them and allows us to verify our program and use its results for the joint analysis of the WTEC and AATR indices. One can see in Fig.2 that for relatively large WTEC$>$0.1TECU, the AATR and WTEC indices correlate well with each other (Fig.2B,J,L,N) and their relation can be described by the proportion:

$$AATR(t)[TECU/min] = 1.5[min^{-1}] \cdot WTEC(t)[TECU] \tag{1}$$

For small WTEC$<$0.1TECU, the correlation between AATR and WTEC is less obvious (Fig.2D,F,H), and the relationship between the indices can be represented as:

$$AATR(t)[TECU/min] \geq 1.5[min^{-1}] \cdot WTEC(t)[TECU] \tag{2}$$

This is an indirect sign that AATR index can be considered as a superposition of the term proportional to WTEC index and additional small term of the order of 0.1TECU, that is significant only for mid-latitude observations where WTEC values are regularly small. The region WTEC<0.1TECU is shown in Fig.2B,J,L,N by dashed line. As one can see in Fig.2, large WTEC values are more often observed at high-latitude and equatorial stations. These latitudes are characterized by higher level of ionospheric disturbances. Therefore, at these stations during strong ionospheric disturbances (for example, generated by geomagnetic storms) one can use both AATR and WTEC indices with equal efficiency. At mid-latitude stations, where the disturbance level is usually lower, one should use a more sensitive index of these two.

4. Sensitivity of the indices to space and surface disturbances

Fig.2 shows that during strong disturbances (corresponding to high AATR and WTEC values) at high-latitudes and low-latitudes AATR and WTEC indices correlate well and are nearly proportional to each other, and using them for analysis is equivalent. For a more detailed analysis of these indices at mid- and high-latitudes, we use the large data set of ISTP SB RAS GNSS stations: mid-latitude SibNet network near the lake Baikal (10 stations) and high-latitude NORI station in the Arctic region. The Baikal region is characterized by significant seismic activity, which makes it possible to estimate the contribution to AATR and WTEC indices the various sources of disturbances, both from the space and from the ground. In Fig.2C,E,G,I,M one can see that the AATR index at mid- and low latitudes has a high level of regular variations. A preliminary spectral analysis shows the presence of a substantial diurnal component in the AATR index, which is less significant in the WTEC index. To study the sources of regular and irregular variations of the indices we estimate regression dependence of WTEC and AATR indices on various parameters of the solar, geomagnetic and seismic activity as well as on background ionospheric conditions as the following:

$$\begin{aligned} WTEC_{fit}(t) &= A_0 + \sum_{i=1}^{4} F_i(t) = A_0 + \sum_{i=1}^{4} A_i I_i(t) \\ AATR_{fit}(t) &= B_0 + \sum_{i=1}^{4} G_i(t) = B_0 + \sum_{i=1}^{4} B_i I_i(t) \end{aligned} \tag{3}$$

Unknown regression coefficients A_i, B_i are calculated by the least squares method to provide the best fit of the experimental measurements $(WTEC(t), AATR(t))$ by the models (3):

$$\begin{aligned} \int_{-\infty}^{\infty} \left(WTEC(t) - WTEC_{fit}(t)\right)^2 dt = min \\ \int_{-\infty}^{\infty} \left(AATR(t) - AATR_{fit}(t)\right)^2 dt = min \end{aligned} \tag{4}$$

The following time series with a temporal resolution 1 hour were used for regression analysis of WTEC and AATR (3-4): $I_1(t)$ is the geomagnetic index Kp; $I_2(t)$ is VTEC, characterizing the background ionospheric conditions obtained from Global Ionosphere Maps (GIM); $I_3(t)$ is F10.7 index of solar activity; $I_4(t)$ is the vertical seismic variation (dZ) according to the data of Talaya seismic station (TLY). When processing to bring all the parameters to the same temporal resolution, rare data (Kp index) are approximated by a step function between measurements, for frequent data the maximum value over 1 hour is taken.

We calculated the relative contribution α_i, β_i of each time series to AATR and WTEC indices as:

$$\begin{aligned} \alpha_i &= \frac{\int_{-\infty}^{\infty} |F_i(t)| dt}{\sum_{j=1}^{4} \int_{-\infty}^{\infty} |F_j(t)| dt} \\ \beta_i &= \frac{\int_{-\infty}^{\infty} |G_i(t)| dt}{\sum_{j=1}^{4} \int_{-\infty}^{\infty} |G_j(t)| dt} \end{aligned} \tag{5}$$

The parameters α_i, β_i are non-negative and dimensionless, and the bigger α_i, β_i the greater the contribution to the index value is made by the disturbance component $I_i(t)$. Thus, the analysis of the parameters α_i, β_i obtained as a result of fitting eq.(4), allows us to identify the main components that regularly affect the behavior of AATR and WTEC indices and to make a comparative analysis of the contribution of each source of disturbances to WTEC and AATR. The calculated parameters α_i, β_i are shown in the Table 1.

The Table 1 shows that at mid-latitude stations the influence of the regular VTEC on WTEC is less than its influence on AATR. WTEC dependence

Table 1: Sensitivity of AATR and WTEC indices to geomagnetic, solar and seismic disturbances according to ISTP SB RAS GNSS stations

Mode	Average over 10 mid-latitude SibNet stations		High-latitude station NORI	
	α_i(WTEC)	β_i(AATR)	α_i(WTEC)	β_i(AATR)
Kp	0.011	0.002	0.734	0.957
VTEC	0.874	0.995	0.262	0.035
F10.7	0.093	0.002	0.004	0.008
dZ	0.022	0.002	0.000	0.000

on intensity of seismic and geomagnetic disturbances is more pronounced than AATR dependency. It should be noted that the small influence of the Kp level at mid-latitude stations may be caused by the weakness of the effects of geomagnetic disturbances at mid-latitudes. The small influence of the seismic activity may be caused by relatively weak seismic activity of the region during the period of observations (maximal magnitude of the seismic events in near-Baikal region was M5.4). At high-latitude NORI station, the dependence on geomagnetic disturbance prevails others both for AATR and for WTEC, which confirms well with the conclusions of (Juan et al., 2018) about the possibility of using the AATR index for analyzing ionospheric disturbances at high latitudes during geomagnetic disturbances. The smallness of effects of VTEC at high latitudes can be related with smaller diurnal variation of VTEC.

5. Case comparison of AATR and WTEC during strong and weak disturbances

To illustrate the sensitivity of AATR and WTEC indices to different disturbances, their responses to some geomagnetic storms and earthquakes were calculated. Geomagnetic storms cause strong disturbances in the ionosphere. Detection and study of these disturbances are one of the practically important applications of indices. Geomagnetic storms on March 17-25 and June 21-30, 2015 are among the strongest storms during 24 solar activity cycle(Liu et al.,

2015). To characterize the geomagnetic field disturbance, we used the Dst (resolution of 1 hour) and SYM-H (resolution of 1 minute) geomagnetic indices. Fig.3A shows the SYM-H and Dst dynamics during the March 17-25, 2015 geomagnetic storm. According to SYM-H, the storm sudden commencement (SSC) was registered at 04:45 UT on March 17. The maximum of the storm was observed at 22:47UT on March 17, when the geomagnetic indices reached their minimum values: SYM-H=-234 nT, Dst=-223 nT (Fig.3A). The geomagnetic field disturbance during the June 21-30, 2015 storm is shown in Fig.3D. SYM-H and Dst dynamics shows SSC at 16:45UT on June 21, 2015 and several peaks during the storm main phase. The main minimum of SYM-H (-206 nT) and Dst (-204 nT) was registered on June 23 at 04:38 UT, after which the long (lasted until June 30) storm recovery phase began (Fig.3D). Fig.3B,E and Fig.3C,F demonstrate the behavior of the AATR and WTEC indices at high-latitude NORI station and at mid-latitude SARM station. As we can see in (Fig.3B,E), WTEC and AATR correlate well during storm time at high-latitudes. At mid-latitudes (Fig.3C,F), the storm effect is more pronounced in WTEC data; in the AATR data the storm generated disturbance is small compared to the quasi-regular daily AATR dynamics.

Earthquakes usually produce less powerful ionospheric disturbances of various types. The basic sources of ionospheric disturbances are internal atmospheric waves generated by seismic vibrations near epicenter (Astafyeva et al., 2013) and shock acoustic waves generated by surface seismic waves near observation point (Berngardt et al., 2017). Fig.4B,D demonstrate AATR and WTEC behavior during the seismic vibrations observed at TLY station and shown in Fig.4A,C. Both WTEC and AATR allow one to detect powerful disturbances, for example after the earthquake in the Aegean Sea on 24/05/2014 09:25UT, about 5800 km from SibNet (Fig.4A-B). On the other hand, WTEC make it possible to register weaker effects than AATR, for example, disturbances observed several hours after the Pacific earthquake of 09/10/2014 02:14UT, about 16500 km from SibNet (Fig.4C-D). Ionospheric response in both cases (marked at Fig.4B,D by arrows) can be related with the passage of internal atmospheric

waves, which can be justified by the presence of significant several hours delay between seismic observation (dashed line) and ionospheric observation (arrow). This delay between them corresponds to atmospheric wave propagation velocity (about 250-350m/s). In the AATR data these disturbances are also present, but less pronounced due to the presence of the diurnal variation of the index. The effect of the earthquake on 23/05/2014 19:43UT at East Baikal looks not observed, which is associated, apparently, with earthquake insufficient magnitude (Perevalova et al., 2014). Thus, the comparison of AATR and WTEC dynamics confirms our conclusion about the higher sensitivity of the WTEC index to weak disturbances as compared to AATR and the lesser influence of the background electron dynamics to WTEC.

6. Conclusion

An important task of monitoring ionospheric disturbances at mid latitudes using single GNSS-receivers is to construct sensitive and effective indices describing the intensity of ionospheric disturbances. One of the widely used indices today is the ROTI index (Pi et al., 1997) and AATR index - its average satellite-receiver beam value averaged over 1 hour (Sanz et al., 2014; Juan et al., 2018). The indices are often used to analyze the high-latitude and equatorial ionosphere, but usually are not used at mid-latitudes. The aim of this paper was to study the efficiency of using the WTEC index obtained with a 30-second time resolution (Voeykov et al., 2016) for analyzing disturbances in the mid-latitude ionosphere based on long-term observations at the complex of mid-latitude GNSS receivers of the ISTP SB RAS and its comparative analysis with the AATR index.

A case comparative analysis of AATR and WTEC indices was performed based on selected GNSS receivers. It is shown that at high and low latitudes at high levels of ionospheric disturbance (when WTEC $>$ 0.1TECU), AATR is proportional to WTEC with a factor of $1.5 min^{-1}$. At mid-latitudes at small levels of ionospheric disturbance (when WTEC $<$0.1TECU), this proportionality

is violated. In this case AATR level becomes higher than expected.

A comparative statistical analysis of AATR and WTEC indices was performed based on ISTP SB RAS mid- and high-latitude GNSS receivers during period 2014-2017. A regression analysis was made with parameters of solar, geomagnetic and seismic activity as well as with background total electron content. It is shown that the contribution of daily dynamics of the background ionosphere to the AATR index is higher than to the WTEC index. This leads to a higher sensitivity of the WTEC index to different disturbances. This also leads to violating the proportionality between WTEC and AATR indices at low levels of ionospheric disturbances. It is shown that at high latitudes the dynamics of the WTEC and AATR indices correlate significantly with the level of geomagnetic disturbance Kp. At mid-latitudes, the contribution of solar radiation variations (F10.7 index) and seismic activity exceeds the influence of Kp variations.

The analysis of strong and weak events associated with geomagnetic disturbances and seismic disturbances demonstrated the higher sensitivity of the WTEC index than AATR at mid latitudes to ionospheric disturbances. Thus, at WTEC $<$0.1TECU, the use of the WTEC index looks more accurate; at high disturbance levels, the WTEC and AATR indices are almost proportional to each other so their use at high and low latitudes looks equivalent. The program for calculating WTEC indices, used in the paper is put into open access (Voeykov and Berngardt, 2019).

Acknowledgments

The authors are grateful to Center for Orbit Determination in Europe for GIM data available on the website ftp://cddis.gsfc.nasa.gov:21/gnss/products/ionex. We are grateful to IRIS/IDA Seismic Network (II), Global Seismograph Network (GSN - IRIS/USGS) (GSN,IU), SY - Synthetic Seismograms Network (SY) for providing seismic data. SibNet from Angara Center for Common Use of scientific equipment (http://ckp-rf.ru/ckp/3056/) is operated under budgetary funding of

Basic Research program II.12. The work was done under support of the joint grant #17-45-388072r_a of RFBR and Goverment of Irkutsk Region, Russia.

References

Afraimovich, E., Edemskiy, I., Voeykov, S., Yasyukevich, Y., Zhivetiev, I., 2009. Spatio-temporal structure of the wave packets generated by the solar terminator. Advances in Space Research 44, 824 – 835. doi:https://doi.org/10.1016/j.asr.2009.05.017.

Afraimovich, E.L., Astafyeva, E.I., Demyanov, V.V., Edemskiy, I.K., Gavrilyuk, N.S., Ishin, A.B., Kosogorov, E.A., Leonovich, L.A., Lesyuta, O.S., Palamartchouk, K.S., Perevalova, N.P., Polyakova, A.S., Smolkov, G.Y., Voeykov, S.V., Yasyukevich, Y.V., Zhivetiev, I.V., 2013. A review of gps/glonass studies of the ionospheric response to natural and anthropogenic processes and phenomena. J. Space Weather Space Clim. 3, A27. doi:10.1051/swsc/2013049.

Astafyeva, E., Shalimov, S., Olshanskaya, E., Lognonné, P., 2013. Ionospheric response to earthquakes of different magnitudes: Larger quakes perturb the ionosphere stronger and longer. Geophysical Research Letters 40, 1675–1681. URL: https://agupubs.onlinelibrary.wiley.com/doi/abs/10.1002/grl.50398, doi:10.1002/grl.50398.

Astafyeva, E., Shults, K., 2018. Ionospheric gnss imagery of seismic source: Possibilities, difficulties, and challenges. Journal of Geophysical Research: Space Physics 0. doi:10.1029/2018ja026107.

Béniguel, Y., Forte, B., Radicella, S.M., Strangeways, H.J., Gherm, V.E., Zernov, N.N., 2004. Scintillations effects on satellite to Earth links for telecommunication and navigation purposes. Annals of Geophysics 47. doi:10.4401/ag-3293.

Berngardt, O.I., Perevalova, N.P., Dobrynina, A.A., Kutelev, K.A., Shestakov, N.V., Bakhtiarov, V.F., Kusonsky, O.A., Zagretdinov, R.V., Zherebtsov,

G.A., 2015. Toward the azimuthal characteristics of ionospheric and seismic effects of "chelyabinsk" meteorite fall according to the data from coherent radar, gps, and seismic networks. Journal of Geophysical Research: Space Physics 120, 10,754–10,771. doi:10.1002/2015JA021549.

Berngardt, O.I., Perevalova, N.P., Podlesnyi, A.V., Kurkin, V.I., Zherebtsov, G.A., 2017. Vertical midscale ionospheric disturbances caused by surface seismic waves based on Irkutsk chirp ionosonde data in 2011-2016. Journal of Geophysical Research: Space Physics 122, 4736–4754. URL: https://agupubs.onlinelibrary.wiley.com/doi/abs/10.1002/2016JA023511, doi:10.1002/2016JA023511.

CDDIS, 2019. Cddis database. URL: ftp://cddis.gsfc.nasa.gov:21/gnss/products/ionex.

Cherniak, I., Krankowski, A., Zakharenkova, I., 2018. Roti maps: a new igs ionospheric product characterizing the ionospheric irregularities occurrence. GPS Solutions 22, 69. doi:10.1007/s10291-018-0730-1.

Gulyaeva, T., Arikan, F., Hernandez-Pajares, M., Stanislawska, I., 2013. Gimtec adaptive ionospheric weather assessment and forecast system. Journal of Atmospheric and Solar-Terrestrial Physics 102, 329 – 340. doi:https://doi.org/10.1016/j.jastp.2013.06.011.

Gulyaeva, T.L., Stanislawska, I., 2008. Derivation of a planetary ionospheric storm index. Annales Geophysicae 26, 2645–2648. doi:10.5194/angeo-26-2645-2008.

Hargreaves, J., 1992. The solar-terrestrial environment. Cambridge University Press. doi:10.1017/cbo9780511628924.

Ho, C.M., Mannucci, A.J., Sparks, L., Pi, X., Lindqwister, U.J., Wilson, B.D., Iijima, B.A., Reyes, M.J., 1998. Ionospheric total electron content perturbations monitored by the gps global network during two northern hemisphere

winter storms. Journal of Geophysical Research: Space Physics 103, 26409–26420. doi:10.1029/98JA01237.

Hofmann-Wellenhof, B., Lichtenegger, H., Collins, J., 2001. Global Positioning System. Springer Vienna. doi:10.1007/978-3-7091-6199-9.

IGS, 2019. Igs database. URL: ftp://garner.ucsd.edu:21/pub/rinex/.

IGS, RTCM-SC104, 2015. Rinex. the receiver independent exchange format. version 3.03. URL: ftp://igs.org/pub/data/format/rinex303.pdf.

IRIS, 2019. Iris database. URL: http://www.ds.iris.edu/ds/.

Ishin, A., Perevalova, N., Voeykov, S., Khakhinov, V., 2017. First results of registering ionospheric disturbances obtained with SibNet network of GNSS receivers in active space experiments. Solar-Terrestrial Physics 3, 74–82. doi:10.12737/stp-34201708.

Jacobsen, K., Andalsvik, Y., 2016. Overview of the 2015 st. patrick´s day storm and its consequences for rtk and ppp positioning in norway. J. Space Weather Space Clim. 6, A9. URL: https://doi.org/10.1051/swsc/2016004, doi:10.1051/swsc/2016004.

Jacobsen, K., Dähnn, M., 2014. Statistics of ionospheric disturbances and their correlation with gnss positioning errors at high latitudes. J. Space Weather Space Clim. 4, A27. doi:10.1051/swsc/2014024.

Jakowski, N., Béniguel, Y., De Franceschi, G., Pajares, M., Jacobsen, K., Stanislawska, I., Tomasik, L., Warnant, R., Wautelet, G., 2012a. Monitoring, tracking and forecasting ionospheric perturbations using GNSS techniques. J. Space Weather Space Clim. 2, A22. doi:10.1051/swsc/2012022.

Jakowski, N., Borries, C., Wilken, V., 2012b. Introducing a disturbance ionosphere index. Radio Science 47. doi:10.1029/2011RS004939.

Jakowski, N., Hoque, M.M., 2019. Estimation of spatial gradients and temporal variations of the total electron content using ground-based gnss measurements. Space Weather 17, 339–356. doi:10.1029/2018SW002119.

Juan, J., Sanz, J., Rovira-Garcia, A., González-Casado, G., Ibáñez, D., Perez, R.O., 2018. Aatr an ionospheric activity indicator specifically based on gnss measurements. J. Space Weather Space Clim. 8, A14. doi:10.1051/swsc/2017044.

Kakinami, Y., Yamamoto, M., Chen, C.H., Watanabe, S., Lin, C., Liu, J.Y., Habu, H., 2013. Ionospheric disturbances induced by a missile launched from north korea on 12 december 2012. Journal of Geophysical Research: Space Physics 118, 5184–5189. doi:10.1002/jgra.50508.

Liu, Y., Hu, H., Wang, R., Yang, Z., Zhu, B., Liu, Y., Luhmann, J., Richardson, J., 2015. Plasma and magnetic field characteristics of solar coronal mass ejections in relation to geomagnetic storm intensity and variability. The Astrophysical Journal 809, L34. doi:10.1088/2041-8205/809/2/l34.

Mannucci, A.J., Wilson, B.D., Yuan, D.N., Ho, C.H., Lindqwister, U.J., Runge, T.F., 1998. A global mapping technique for GPS-derived ionospheric total electron content measurements. Radio Science 33, 565–582. doi:10.1029/97RS02707.

Mendillo, M., Lin, B., Aarons, J., 2000. The application of gps observations to equatorial aeronomy. Radio Science 35, 885–904. doi:10.1029/1999RS002208.

Nesterov, I.A., Andreeva, E.S., Padokhin, A.M., Tumanova, Y.S., Nazarenko, M.O., 2017. Ionospheric perturbation indices based on the low- and high-orbiting satellite radio tomography data. GPS Solutions 21, 1679–1694. doi:10.1007/s10291-017-0646-1.

OMNIWeb, 2019. Omniweb database. URL: https://omniweb.gsfc.nasa.gov/form/dx1.html.

Perevalova, N., Edemsky, I., Timofeeva, O., Katashevtseva, D., Yasyukevich, A., 2016. Dynamics of disturbance level of total electron content at high and middle latitudes according to gps data. Solnechno-Zemnaya Fizika 2, 36–43.

Perevalova, N., Sankov, V., Astafyeva, E., Zhupityaeva, A., 2014. Threshold magnitude for ionospheric tec response to earthquakes. Journal of Atmospheric and Solar-Terrestrial Physics 108, 77 – 90. doi:https://doi.org/10.1016/j.jastp.2013.12.014.

Perevalova, N.P., Afraimovich, E.L., Voeykov, S.V., Zhivetiev, I.V., 2008. Parameters of large-scale tec disturbances during the strong magnetic storm on 29 october 2003. Journal of Geophysical Research: Space Physics 113. doi:10.1029/2008JA013137.

Pi, X., Mannucci, A.J., Lindqwister, U.J., Ho, C.M., 1997. Monitoring of global ionospheric irregularities using the worldwide gps network. Geophysical Research Letters 24, 2283–2286. doi:10.1029/97GL02273.

Polyakova, A., Perevalova, N., 2013. Comparative analysis of tec disturbances over tropical cyclone zones in the northâĂŞwest pacific ocean. Advances in Space Research 52, 1416 – 1426. doi:https://doi.org/10.1016/j.asr.2013.07.029.

Sanz, S., Juan Z., J.M., C.G., G., C.R., P., Schlueter, S., P.R., O., et al., 2014. Novel ionospheric activity indicator specifically tailored for GNSS users, The Institute of Navigation, Proceedings of ION GNSS+. Tampa, Florida (USA). pp. 1173–1182.

Stanislawska, I., Gulyaeva, T., 2015. Ionospheric W Index Based on GNSS TEC in the Operational Use for Navigation Systems. doi:10.5772/59902.

Stankov, S.M., Jakowski, N., Tsybulya, K., Wilken, V., 2006. Monitoring the generation and propagation of ionospheric disturbances and effects on Global Navigation Satellite System positioning. Radio Science 41. doi:10.1029/2005RS003327.

Voeykov, S., Berngardt, O., 2019. berng/wtec: Wtec v.1.0.1. URL: https://zenodo.org/record/2604418, doi:10.5281/ZENODO.2604418.

Voeykov, S.V., Berngardt, O.I., Shestakov, N.V., 2016. Use of the index of tec vertical variation disturbance in studying ionospheric effects of the chelyabinsk meteorite. Geomagnetism and Aeronomy 56, 219–228. doi:10.1134/S0016793216020122.

Wanninger, L., 1993. Ionospheric monitoring using igs data, Proceedings of the 1993 IGS Workshop Berne, Switzerland: Astronomical Institute, Univ. of Berne. pp. 351–360.

WDC, K., 2019. Kyoto wdc database. URL: http://wdc.kugi.kyoto-u.ac.jp/.

Wilken, V., Kriegel, M., Jakowski, N., Berdermann, J., 2018. An ionospheric index suitable for estimating the degree of ionospheric perturbations. J. Space Weather Space Clim. 8, A19. doi:10.1051/swsc/2018008.

Zherebtsov, G.A., Perevalova, N.P., 2019. Gnss potential to monitor unsuccessful spacecraft launches. GPS Solutions 23, 30. doi:10.1007/s10291-018-0822-y.

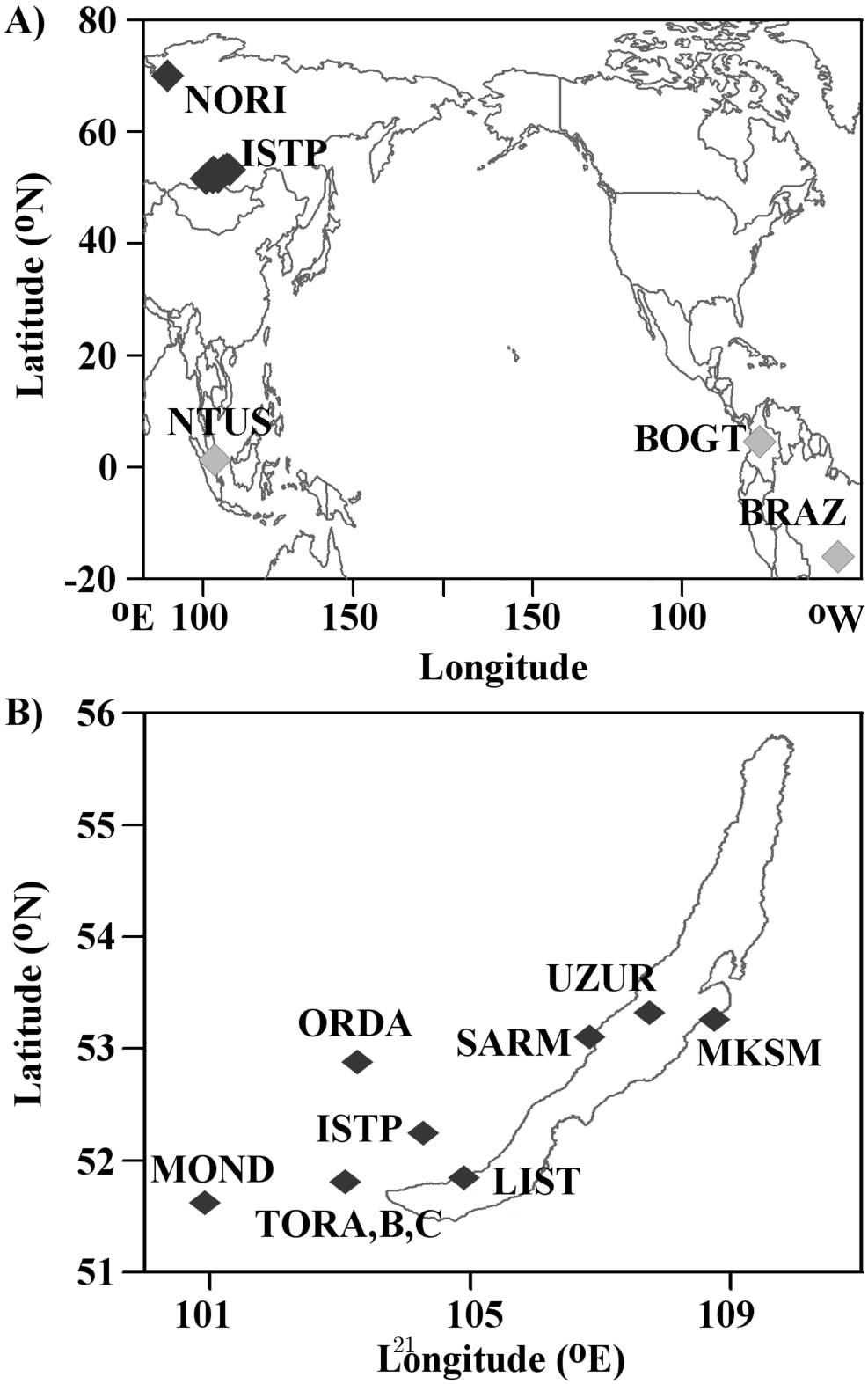


Figure 1: Location of all GNSS stations used in this paper (A), ISTP SB RAS stations near lake Baikal (B). The black and gray rhombs mark the GNSS stations of ISTP SB RAS and IGS, correspondingly.

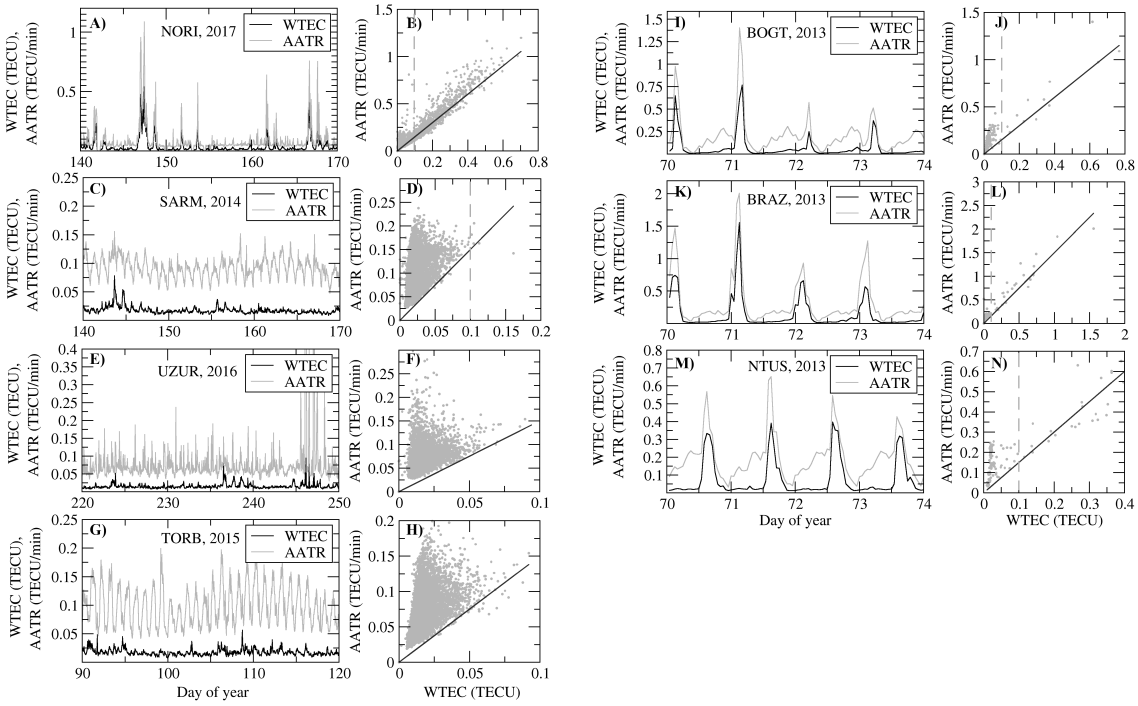


Figure 2: Comparison of AATR (gray line) and WTEC (black line) indices dynamics based on the data from various stations - high-latitude (A-B), mid-latitude (C-H) and low-latitude (I-N) ones. Left panels correspond to the dynamics of indices and right panels correspond to regression dependence of AATR on WTEC. Gray points are experimental points, the solid line corresponds to the regression dependence (1). Vertical dashed line limits the region WTEC$<$0.1TECU.

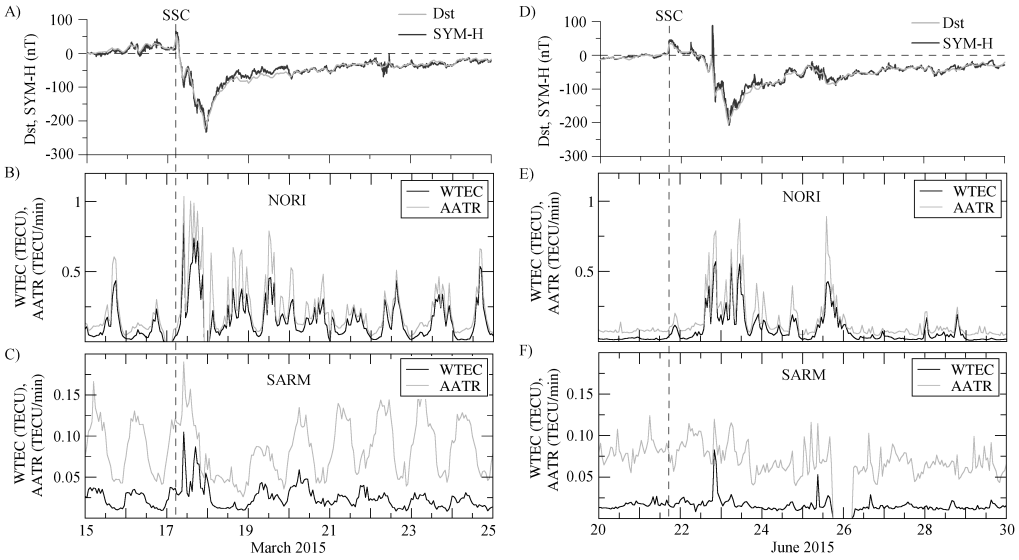


Figure 3: AATR and WTEC dynamics at high-latitude (NORI) and mid-latitude (SARM) ISTP SB RAS GNSS-stations during March 15-25, 2015 (A-C) and June 20-30, 2015 (D-F) geomagnetic storms. The vertical dashed line marks the SSC. A, D) - Dst and SYM-H; B,E) - WTEC and AATR at NORI; C,F) - WTEC and AATR at SARM.

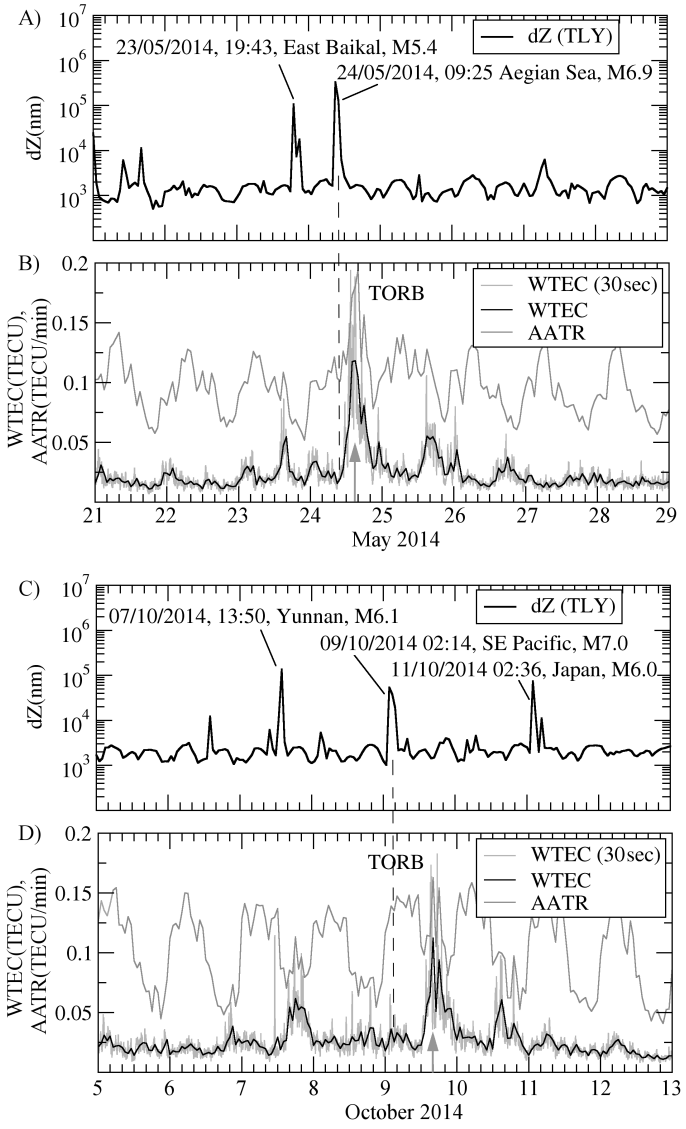


Figure 4: AATR and WTEC dynamics during seismic disturbances. A,C) - data of the Talaya seismic station (TLY). B,D) - TORB GNSS-receiver data. The light gray line corresponds to WTEC with 30-second temporal resolution, the black and dark gray lines mark, respectively, WTEC and AATR with 1 hour temporal resolution. Vertical dashed line marks the earthquake vibrations received at TLY station. Arrow marks the ionospheric response possibly related with it.